Neuron, Vol. 19, 913–926, October, 1997, Copyright ©1997 by Cell Press

Identification of Amino Acid Residues that Control Functional Behavior in GluR5 and GluR6 Kainate Receptors

Geoffrey T. Swanson,* Robert W. Gereau IV, Tim Green, and Stephen F. Heinemann
Molecular Neurobiology Laboratory
The Salk Institute
10010 North Torrey Pines Road
La Jolla, California 92037

Summary

GluR5 and GluR6 kainate receptors differ in their responses to a variety of agonists, despite their relatively high primary sequence homology. We carried out a structure–function study to identify amino acids underlying these divergent responses. Patch clamp analysis of chimeric GluR5-GluR6 receptors indicated that several functionally dominant sites were localized to the C-terminal side of M1. All nonconserved amino acids in the region between M3 and M4 of GluR6 were then individually mutated to their GluR5 counterparts. We found that a single amino acid (N721 in GluR6) controls both AMPA sensitivity and domoate deactivation rates. Additionally, mutation of A689 in GluR6 slowed kainate desensitization. These functional effects were accompanied by alterations in binding affinities. These results support a critical role for these residues in receptor binding and gating activity.

Introduction

Ionotropic glutamate receptor subunits constitute a large family of ligand-gated ion channels responsible for the majority of excitatory synaptic transmission in the central nervous system. This gene family is subdivided into non-NMDA and NMDA receptor subunits, which underlie the fast and slow component of excitatory transmission, respectively. Characterization of the nine cloned non-NMDA receptor subunits has identified two subfamilies, α-amino-3-hydroxy-5-methyl-4-isoxazolepropionic acid (AMPA) preferring (GluR1–4) and kainate preferring (GluR5–7, KA-1 and KA-2) (Hollmann and Heinemann, 1994). Despite ~40% amino acid sequence homology, AMPA receptor subunits do not coassemble with kainate receptors (Brose et al., 1994; Patneau et al., 1994; Puchalski et al., 1994; Wenthold et al., 1994), and these receptor subfamilies exhibit different agonist affinities and response kinetics (Hollmann and Heinemann, 1994). However, expression and functional characterization of cloned AMPA and kainate receptors have revealed a strong similarity in their response to the endogenous neurotransmitter glutamate. All functional non-NMDA subunits cloned to date respond to fast applied glutamate at high concentration (mimicking synaptic transmission) with rapid activation and desensitization (Sommer et al., 1992; Köhler et al., 1993; Mosbacher et al., 1994). In contrast, other agonists elicit quite distinct currents from AMPA and kainate receptors (Sommer et al., 1990; Sommer et al., 1992; Köhler et al., 1993). In combination with differential sensitivities to allosteric modulators such as cyclothiazide, concanavalin A, and GYKI 53655 (Partin et al., 1993; Wilding and Huettner, 1995), this divergent pharmacology has proven useful for identifying receptor types underlying responses in neurons and glia (Lerma et al., 1993; Partin et al., 1993; Patneau et al., 1994; Puchalski et al., 1994; Wilding and Huettner, 1997).

Agonist-binding affinities and response characteristics also have been used as a tool for exploring the membrane topology and agonist-binding domain of non-NMDA receptors. A divergence in function and agonist sensitivity of AMPA and kainate receptors is observed with agonists such as AMPA, kainate, and domoate (Hollmann and Heinemann, 1994). Using agonist-binding affinities of GluR3-GluR6 chimeric subunit proteins, Stern-Bach et al. (1994) mapped the ligand-binding domain to two regions they termed S1 and S2, which precede M1 and follow M3, respectively. Their results supported other studies that proposed a new topology for glutamate receptors that modeled the second hydrophobic region as a reentrant loop rather than a membrane-spanning helix (Hollmann et al., 1994; Wo and Oswald, 1994; Bennett and Dingledine, 1995). This model therefore predicts that the region between the end of M3 and the beginning of M4, which includes the S2 domain, is located on the extracellular side of the plasma membrane. While the GluR3-GluR6 chimeras identified macrodomains involved in binding, interpretation of changes to agonist response kinetics was problematic in these cross-family (AMPA/kainate) chimeras, particularly since a number of chimeras were nonfunctional (Stern-Bach et al., 1994). Screening of the agonist-binding domain of glutamate receptors using site mutagenesis has also determined that a limited number of amino acids in the S1 and S2 regions control binding affinity to NMDA receptors and chick kainate-binding proteins (KBP) (Kuryatov et al., 1994; Paas et al., 1996; Laube et al., 1997).

In the current study, we have examined residues involved in both binding and gating by making receptor chimeras and restricted amino acid mutations to two highly homologous kainate receptor subunits, GluR5 and GluR6. These subunits are 80% identical at the amino acid level, with the least conserved domains found in the N- and C-terminal regions (Bettler et al., 1990; Egebjerg et al., 1991). While the responses to glutamate are qualitatively similar in these subunits, those to kainate, AMPA, and the high affinity agonist domoate are quite distinct (Sommer et al., 1992; Köhler et al., 1993). GluR5 receptors desensitize slowly in the presence of kainate, while GluR6 receptors show rapid and nearly complete desensitization. With domoate, both desensitization rates and current decay rates after removal of agonist differ between GluR5 and GluR6. Finally, GluR5 is activated by high concentrations of AMPA, whereas GluR6 is completely insensitive to this compound. These differences in agonist response characteristics were used as an assay for localization of

*To whom correspondence should be addressed.

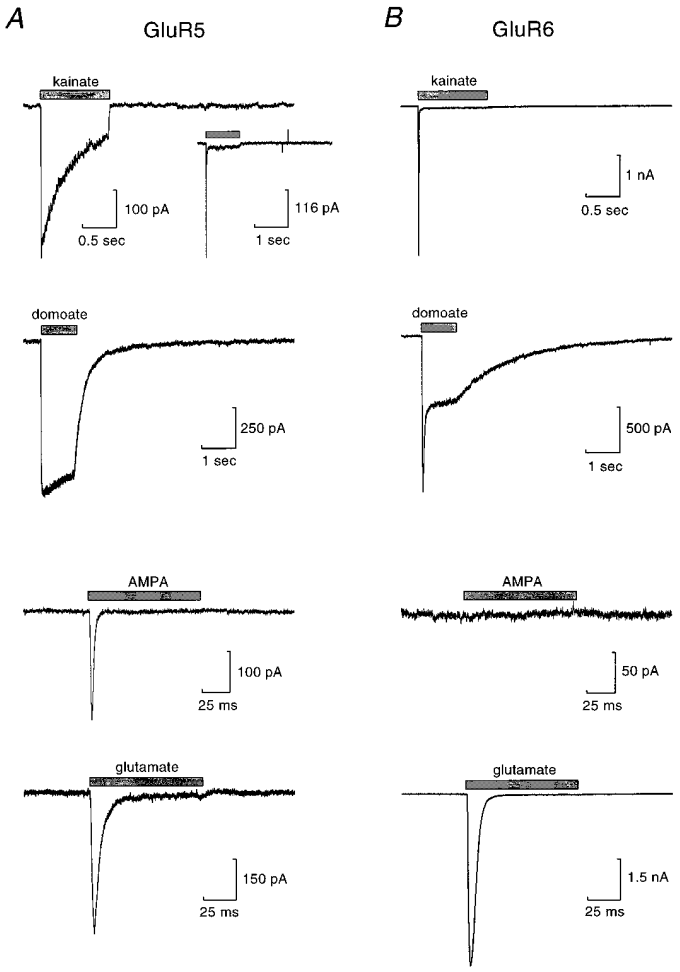

Figure 1. Comparison of Representative Agonist-Evoked Currents from GluR5 (A) and GluR6 (B) Receptors

The inset response in (A) is an example of a fast desensitizing kainate response in GluR5; this type of response was relatively rare. Drugs were applied during the time indicated by the gray bar under the following conditions: 1 mM kainate for 1 s, 30 μM domoate for 1 s, 500 μM AMPA for 100 ms, and 1 mM glutamate for 100 ms. The holding potential was −70 mV in each case.

residues that play a role in binding and/or gating processes in these receptors. We initially constructed chimeras to localize important domains of the proteins that regulate channel kinetics, then proceeded with single and multiple site mutation of amino acids that vary among the subunits. Fast application of agonists allowed us to resolve nondesensitized peak currents and construct a detailed description of the kinetic behavior of the receptor chimeras and mutants. We report the characterization of two sites that control aspects of binding and functional properties of GluR5 and GluR6 kainate receptors.

Results

We first characterized those channel properties that would be useful for mapping the binding and gating domains in GluR5 and GluR6 by analyzing their current kinetics after expression in HEK 293 cells. Consistent with previous reports, we found that GluR5 and GluR6 differ in aspects of their responses to kainate, domoate, and AMPA (Figure 1 and Table 1) (Sommer et al., 1992; Köhler et al., 1993). In GluR5-expressing cells, kainate (1 mM) activated currents with extremely variable desensitization rates (τ_{des} values ranged from 1.5 ms to >3 s; n = 18). An example of a slowly desensitizing kainate response is shown in Figure 1A. This type of response is representative of the majority of kainate-evoked currents we observed in GluR5-expressing cells, in that a mixture of both fast and slow components was observed; the slower desensitizing component predominated in all but a few examples. Three cells (out of 18) showed a predominant fast desensitizing component like that shown in the inset kainate response in Figure 1A (τ_{fast} = 1.4 ms and τ_{slow} = 17.2 ms for inset response). The mechanism that underlies the variability in the GluR5 response to kainate remains unclear. In contrast, kainate consistently evoked rapidly desensitizing currents from GluR6 receptors (τ = 4.4 ± 0.3 ms [mean ± SEM]; n = 11; Figure 1B); steady-state currents were 1.22% ± 0.03% of peak currents with this agonist. Domoate activates slowly desensitizing currents in GluR5 channels and rapidly desensitizing currents in GluR6 but, more interestingly, has an ~7-fold slower deactivation rate in GluR6 compared to GluR5 (Figures 1A and 1B). The decay rates of the currents after removal of domoate were best fitted with two exponential components for both receptors: for GluR5, τ_1 = 0.15 ± 0.11 s and τ_2 = 0.65 ± 0.24 s (relative proportions of 58.4% and 41.6%; n = 9), whereas for GluR6, τ_1 = 1.05 ± 0.1 s and τ_2 = 4.79 ± 0.48 s (relative proportions of 60.7% and 39.3%; n = 12). AMPA does not gate currents in homomeric GluR6, whereas GluR5 has low but detectable sensitivity to AMPA (mean current amplitude with 500 μM AMPA

Table 1. Functional Properties of Kainate Receptors, Chimeras, and GluR6 Site Mutants

	Kainate		Glutamate		Domoate			AMPA
Receptor	i_{peak} (nA)	τ_{des} (ms)	i_{peak} (nA)	τ_{des} (ms)	i_{peak} (nA)	$\tau_{dec}1$ (sec)	$\tau_{dec}2$ (sec)	i_{peak} (pA)
GluR5	0.57 ± 0.08 (18)	variable	0.63 ± 0.16 (5)	4.1 ± 0.9	0.33 ± 0.07	0.15 ± 0.11 (9)	0.65 ± 0.24	111 ± 45 (5)
GluR6	3.4 ± 0.6 (12)	4.4 ± 0.3	4.4 ± 1.0 (9)	4.1 ± 0.2	1.5 ± 0.3	1.05 ± 0.10 (12)	4.79 ± 0.48	ND (13)
R6tm1R5	0.75 ± 0.20 (10)	variable	0.53 ± 0.14 (10)	8.3 ± 1.1	0.39 ± 0.11	0.21 ± 0.03 (9)	0.79 ± 0.09	52 ± 10 (9)
R5tm1R6	0.45 ± 0.08 (7)	2.1 ± 0.2	0.53 ± 0.14 (6)	3.3 ± 0.7	0.13 ± 0.12	0.33 ± 0.08 (7)	ND	ND (8)
R6(E686R)	1.8 ± 0.4 (9)	4.4 ± 0.5	1.9 ± 0.3 (7)	4.8 ± 0.5	0.80 ± 0.21	1.03 ± 0.23 (8)	5.50 ± 1.31	ND (9)
R6(A689S)	3.2 ± 2.2 (8)	***10.2 ± 1.4***	3.5 ± 2.3 (6)	5.8 ± 1.4	1.6 ± 1.4	0.93 ± 0.39 (8)	3.68 ± 1.56	ND (8)
R6(D703E)	3.0 ± 0.5 (6)	4.1 ± 0.3	3.7 ± 0.4 (5)	4.4 ± 0.6	1.6 ± 0.3	1.03 ± 0.12 (5)	4.45 ± 0.45	ND (6)
R6(R713Q)	4.3 ± 0.5 (9)	5.0 ± 0.3	4.9 ± 0.5 (8)	5.9 ± 0.5	1.4 ± 0.4	0.75 ± 0.09 (8)	3.42 ± 0.58	ND (9)
R6(V716A)	2.8 ± 0.4 (7)	4.6 ± 0.5	2.7 ± 0.3 (5)	5.2 ± 0.9	0.72 ± 0.14	0.85 ± 0.07 (7)	4.02 ± 0.41	ND (6)
R6(S720N)	5.0 ± 0.8 (9)	5.2 ± 0.6	5.6 ± 0.9 (8)	5.3 ± 0.7	3.2 ± 0.7	1.04 ± 0.13 (9)	5.53 ± 1.14	ND (6)
R6(N721S)	3.3 ± 0.5 (11)	4.9 ± 0.4	3.4 ± 0.6 (7)	3.5 ± 0.3	1.2 ± 0.3	***0.22 ± 0.03*** (8)	***1.33 ± 0.36***	***287 ± 108*** (11)
R6(E722D)	3.9 ± 0.7 (9)	5.0 ± 0.3	1.8 ± 0.6 (8)	3.4 ± 0.2	1.2 ± 0.3	0.86 ± 0.07 (9)	3.76 ± 0.58	ND (9)
R6(S731T)	2.9 ± 0.5 (10)	4.1 ± 0.2	3.5 ± 0.5 (6)	4.2 ± 0.2	1.1 ± 0.2	1.32 ± 0.18 (8)	4.28 ± 0.61	ND (10)
R6(F735L)	1.6 ± 0.4 (11)	***6.8 ± 0.7***	2.7 ± 1.1 (5)	6.0 ± 0.9	0.49 ± 0.12	***0.62 ± 0.07*** (10)	***2.64 ± 0.45***	ND (8)
R6(T741S)	3.6 ± 0.5 (6)	4.6 ± 0.5	5.2 ± 1.3 (4)	4.3 ± 0.1	1.1 ± 0.3	1.50 ± 0.14 (5)	7.63 ± 1.35	ND (5)
R6(F744Y)	3.4 ± 0.5 (7)	4.4 ± 0.5	3.7 ± 0.7 (5)	4.3 ± 0.4	1.8 ± 0.2	1.49 ± 0.10 (8)	6.42 ± 0.55	ND (6)
R6(M770I)	2.7 ± 0.5 (9)	3.7 ± 0.3	3.5 ± 0.8 (5)	3.5 ± 0.9	2.3 ± 0.6	1.25 ± 0.26 (7)	5.13 ± 0.68	ND (9)
R6(E808D)	2.9 ± 0.4 (6)	3.3 ± 0.3	3.4 ± 0.3 (6)	3.3 ± 0.2	1.6 ± 0.4	0.91 ± 0.11 (8)	3.76 ± 0.58	ND (8)
R6(Q818E)	3.6 ± 0.7 (5)	4.1 ± 0.3	3.6 ± 0.7 (5)	3.9 ± 0.3	2.1 ± 0.5	1.11 ± 0.10 (6)	5.02 ± 0.79	ND (6)
R6(689/721)	3.8 ± 0.4 (8)	***8.1 ± 0.9***	3.6 ± 0.5 (8)	4.5 ± 0.6	3.1 ± 1.0	***0.30 ± 0.05*** (6)	***1.31 ± 0.33***	***81 ± 41*** (3)

All receptors were expressed in HEK 293 cells, and currents were recorded using whole-cell patch clamp. For each receptor and agonist application, the number of cells is shown in parentheses under the mean and SEM values. For the R6 mutants, kinetic properties that are statistically different ($p < 0.05$) from those of GluR6 are shown in bold italics.

was 111 ± 45 pA; n = 5). On GluR5, AMPA also activated currents with variable desensitization kinetics. Glutamate activated rapidly desensitizing currents in both receptor types (GluR5, 4.1 ± 2.0 ms; n = 5; GluR6, 4.1 ± 0.2 ms; n = 9). While the mechanisms underlying the striking variability of GluR5 desensitization rates are unclear, our observations are similar to those recently reported for glutamate-activated GluR6 currents in outside-out patches (Heckmann et al., 1996; Bufler et al., 1997). Because of the variability in GluR5 desensitization rates observed with kainate, we chose to focus primarily on the differences in AMPA sensitivity and domoate deactivation rates as diagnostic assays for important functional domains of the receptors.

Functional Properties of Kainate Receptor Chimeras

Two chimeric kainate receptor subunits were constructed to resolve whether determinants of the divergent agonist responses could be specifically associated with either the N- or C-terminal half of the receptor proteins. Chimera R6tm1R5 was composed of GluR6 sequence up to the start of M1, followed by GluR5 sequence through to the C terminus (Figure 2A). The isoform of GluR5 utilized to construct the chimera was GluR5–2a (Sommer et al., 1992). The R6tm1R5 construct therefore had an S1 domain from GluR6 and an S2 domain from GluR5. The converse arrangement of subunit sequence was generated in chimera R5tm1R6, in which the N-terminal half of GluR5 was spliced onto the C-terminal half of GluR6 (Figure 2B). All receptors and chimeras had a glutamine at the Q/R site in the reentrant loop region (denoted M2). Each chimera was tested for responses to four agonists at single concentrations: 500 μM AMPA, 30 μM domoate, 1 mM kainate, and 1 mM glutamate. Both chimeras expressed functional channels in HEK 293 cells (Figures 2A and 2B).

R6tm1R5 produced channels with currents similar but not identical to those of GluR5 for AMPA, domoate, and kainate (Figure 2A). The channel was sensitive to AMPA,

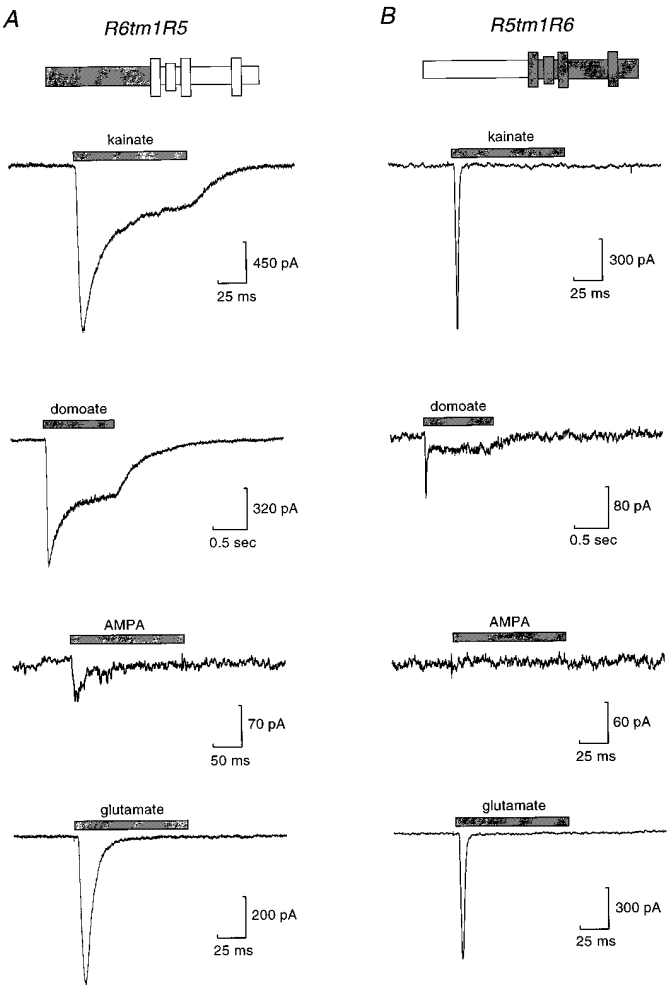

Figure 2. Comparison of Representative Agonist-Evoked Currents from Chimeras R6tm1R5 (A) and R5tm1R6 (B)

The orientations of the chimeras are shown in the cartoons above the corresponding responses. GluR5 domains are represented in white and GluR6 in gray, and membrane-spanning domains are shown as larger boxes. Drugs were applied during the time indicated by the gray bar under the following conditions: 1 mM kainate for 100 ms, 30 μM domoate for 1 s, 500 μM AMPA for 200 ms (GluR5) or 1 mM AMPA for 100 ms (GluR6), and 1 mM glutamate for 100 ms. The holding potential was −70 mV in each case.

responding with a small, desensitizing current (52 ± 10 pA; n = 9). Domoate elicited a desensitizing current with a deactivation rate that was best fitted with two exponential components (τ_1 = 0.21 ± 0.03 s and τ_2 = 0.79 ± 0.09 s; n = 9). These values are not significantly different from those of GluR5 (p = 0.20, unpaired t test). In nine cells, R6tm1R5 kainate currents desensitized somewhat faster than seen for GluR5 but were still an order of magnitude slower than GluR6 kainate desensitization (e.g., compare kainate currents in Figures 1 and 2). Lastly, 1 mM glutamate gave a rapidly activating and desensitizing current with variable kinetics (mean 8.3 ± 1.1 ms; n = 10).

Chimera R5tm1R6 gave channels whose functional properties were similar to those of GluR6 (Figure 2B) with some differences in the responses to glutamate and kainate. No AMPA-evoked currents were detected in eight cells transfected with this chimera (tested at 1 mM AMPA). Both kainate and glutamate gave rapidly desensitizing currents. The kainate desensitization rate for R5tm1R6 was significantly faster than that of GluR6 (τ = 2.1 ± 0.2 ms; n = 7 versus 4.4 ± 0.3 ms; p < 0.01). The R5tm1R6 glutamate desensitization rate had a τ of 3.3 ± 0.7 ms (n = 6) as compared to 4.1 ± 0.2 ms for GluR6 (not significantly different; p = 0.20). These R5tm1R6 desensitization kinetics are likely to be somewhat slower than the actual rates due to technical limitations in the rate at which we can apply the agonists (10%–90% rise times of the R5tm1R6 currents were 1.1 ± 0.1 ms with kainate and 1.5 ± 0.2 ms for glutamate). Domoate gave very small responses with variable desensitization kinetics in R5tm1R6. Because of the small amplitude of the currents, the deactivation kinetics were difficult to analyze, and time constants were likely to be underestimated. Only a single exponential component could be fitted to the data (τ = 0.33 ± 0.08 s; n = 7).

The functional behavior of these M1 chimeras gives at least one clear example of delineation of agonist properties by a single half of the receptor protein: that of low affinity AMPA sensitivity. AMPA sensitivity appears to correlate with the subunit type comprising the S2 domain of the kainate receptors. While these chimeras do not exclude participation of residues further downstream than S2, strong evidence suggests that S2 is critical for determining the binding properties of ionotropic glutamate receptors (Stern-Bach et al., 1994). We therefore focused on amino acid residues in the S2 region as possible determinants of the functional differences between GluR5 and GluR6.

Control of Kainate Receptor AMPA Sensitivity by a Single Residue in the S2 Domain

In the region between M3 and M4, GluR5 and GluR6 share 91% identity in their amino acid sequence. In order

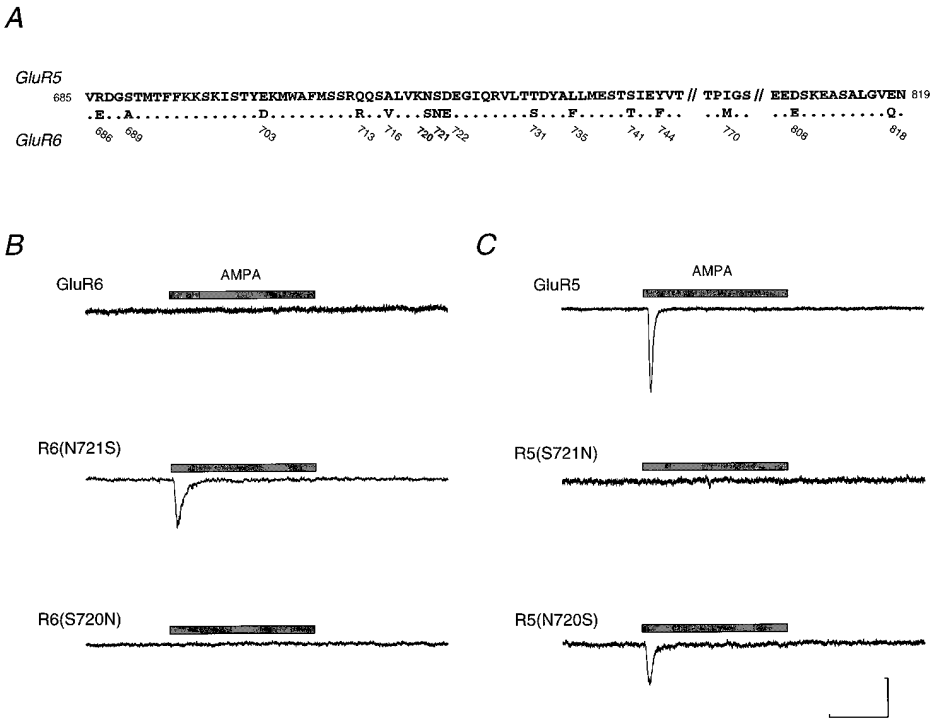

Figure 3. Comparison of GluR5 and GluR6 Amino Acid Sequences in the Region of the Subunit Proteins between M3 and M4 (A) and AMPA Currents in GluR5, GluR6, and Selected Mutants (B and C)

(A) A sequence alignment of GluR5 and GluR6, with only those residues in GluR6 that differ from GluR5 shown on the lower line. The numbering is from the start of the signal peptide. Two regions of complete homology have been omitted. The numbers in bold (720 and 721) indicate sites of mutation for the currents shown in the bottom panel.

(B) Currents evoked by application of AMPA to HEK cells expressing GluR6, R6(N721S), and R6(S720N).

(C) Currents evoked by application of AMPA to HEK cells expressing GluR5, R5(S721N), and R5(N720S). The gray bars mark the 200 ms applications. The AMPA concentration was 500 μM in most cases and 1 mM for R5(S721N). The holding potential was −70 mV in each case. The calibration bars are: x-axis, 40 ms for GluR6, R6(S720N), GluR5, R5(S721N), and R5(N720S) and 80 ms for R6(N721S); y-axis, 150 pA for all traces.

to determine which specific residue(s) in this domain underlie the differing sensitivity to AMPA, we made single-site mutations to all 15 nonconserved amino acids to convert the native GluR6 amino acid to the corresponding GluR5 residue. Selected GluR5 mutants were also made to test whether alterations in current kinetics resulting from GluR6 mutations had reciprocal effects on GluR5. In reporting these results, we have numbered amino acids in GluR5 and GluR6 starting with their signal peptides; note also that GluR5–2a does not contain the N-terminal insertion as reported in GenBank (see Experimental Procedures). All single- and multiple-site GluR6 and GluR5 mutants were tested with the same battery of agonists as used with the chimeras, and all site mutants were functional.

As shown in Table 1, a single GluR6 S2 site mutant, R6(N721S), was sensitive to AMPA. All other GluR6 site mutants failed to gate currents during fast application of 500 μM AMPA. R6(N721S) had AMPA-gated currents with a mean amplitude of 287 ± 108 pA (n = 11). Figure 3B shows example traces of AMPA application to native GluR6, R6(N721S), and its neighboring mutation site, R6(S720N). The AMPA currents activated slowly compared to kainate and glutamate (10%–90% rise time of 3.3 ± 0.3 ms for AMPA and 1.2 ± 0.1 ms for kainate and glutamate), most probably because the concentration of AMPA used was lower than the peak EC_{50}, which has been estimated at 3 mM for GluR5 (Sommer et al., 1992). The peak AMPA current seen for R6(N721S) was 8.0% ± 2.5% of the peak glutamate current in cells where both agonists were tested (n = 7), as compared to 17.6% ± 3.6% in GluR5 (n = 5). R6(N721S) AMPA currents predominantly desensitized with a $\tau \approx 12$ ms, but these kinetics showed a great deal of variability. Two cells had a double exponential desensitization rate with a slower $\tau > 100$ ms. These current characteristics are similar to those seen when AMPA is applied to GluR5 and differ considerably from the AMPA currents gated by GluR6/KA-2 heteromers (Herb et al., 1992), which consistently desensitize very slowly.

From the analysis of the GluR6 mutants, it appeared that amino acid N721 was the primary determinant of AMPA sensitivity in kainate receptors. If this is the case, then the complementary serine-to-asparagine mutation in GluR5 should eliminate AMPA-gated currents. As shown in Figure 3C and Table 1, R5(S721N) was insensitive to AMPA (n = 6) (middle trace, Figure 3C), while its neighboring mutation, R5(N720S), showed no significant reduction in AMPA currents as compared to native GluR5 (top and bottom traces, Figure 3C). Thus, S721 seems to be necessary to generate low affinity AMPA currents in these kainate receptors.

Amino Acid N721 Also Controls the Rate of Channel Deactivation after Application of Domoate

R6(N721S) responses to domoate also exhibited a deactivation rate that was closer to that of GluR5 (Figures 4A and 4B), while the domoate desensitization rate and

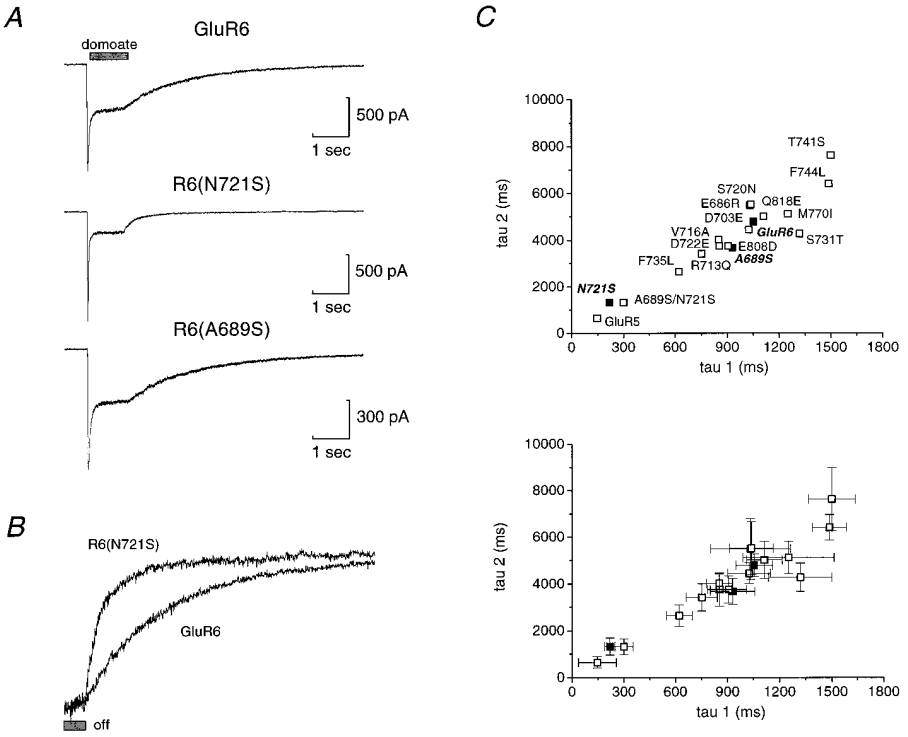

Figure 4. Domoate-Evoked Currents in GluR6 and Mutants (A and B) and Comparison of Deactivation Rates for GluR5, GluR6, and all GluR6 Mutants (C)

(A) Currents evoked by application of 30 μM domoate to HEK cells expressing GluR6, R6(N721S), and R6(A689S). The holding potential was −70 mV in each case.

(B) Comparison of deactivation rates after removal of domoate from GluR6 and R6(N721S) traces shown in (A). The deactivation rate constants for the currents shown were 0.24 and 1.45 s for R6(N721S) and 1.33 and 5.89 s for GluR6.

(C) Plot of the mean fast versus slow deactivation rate constants for GluR5, GluR6, and all GluR6 mutants; in the top panel, the mutants are identified, and in the bottom, the SEM bars are shown. GluR6, R6(N721S), and R6(A689S) are shown as closed squares and highlighted in bold.

glutamate and kainate responses were similar to that of GluR6 (Table 1). The R6(N721S) current decay rate after removal of domoate was best fitted with two exponential components: $\tau_1 = 0.22 \pm 0.03$ s and $\tau_2 = 1.33 \pm 0.36$ s (representing 58% and 42% of the exponential decay, respectively; $n = 8$). This is significantly different from the domoate deactivation from GluR6 ($p < 0.005$) but not statistically different from GluR5 deactivation rates ($p = 0.154$). Figure 4A shows examples of domoate application to native GluR6, R6(N721S), and R6(A689S), and deactivation currents are shown on an expanded scale in Figure 4B. As is apparent from the figure, desensitization rates are relatively unchanged in R6(N721S), but the current decays much faster after removal of domoate. R6(A689S) was of interest, as it exhibits slowed desensitization rates during application of kainate but no alteration in its response to domoate, glutamate, or AMPA (see Figure 6). Domoate deactivation rates for the double mutant R6(A689S/S721N) were indistinguishable from R6(N721S) (data not shown) as were its fast desensitizing AMPA responses, demonstrating that amino acid N721 controls aspects of the kinetic response to domoate.

The time course of receptor deactivation after removal of domoate (subsequent to a prolonged application) reflects the closure of open channels that are in equilibrium with one or more closed states and is also affected by the rate at which ligand unbinds from the receptor complex. For both R5 and R6, this deactivation rate was best fitted as a multiexponential process. To illustrate the clear separation of the R6-type mutants from the R5-like mutants, in Figure 4C we have plotted the slower versus faster mean τ values for GluR5, GluR6, and all the GluR6 mutants. (In the figure, the top graph identifies the mutants, and the bottom graph shows the SEM associated with each data point). R6(N721S) and the double mutant R6(N721S/A689S) were the only two mutants that had deactivation rate components that were both significantly different from GluR6 and indistinguishable from GluR5. An additional mutant, R6(F735L), had a domoate deactivation rate intermediate to that of R5 and R6 ($\tau_1 = 0.62 \pm 0.07$ s and $\tau_2 = 2.64 \pm 0.45$ s; $n = 10$); both exponential components were significantly different than GluR5 and GluR6 ($p < 0.05$). R6(F735L) currents were on average ~50% smaller than currents from GluR6 and other mutants. As is evident from the figure, there is a strong linear relationship between the fast and slow deactivation components of the kainate receptor mutants ($r = 0.95$).

Domoate deactivation kinetics in R5(S721N), the GluR5 mutant complementary to R6(N721S), were significantly slower than native GluR5. Figure 5A shows examples of responses from GluR5 and three mutants: R5(S721N), the complementary mutation to R6(N721S), R5(S689A),

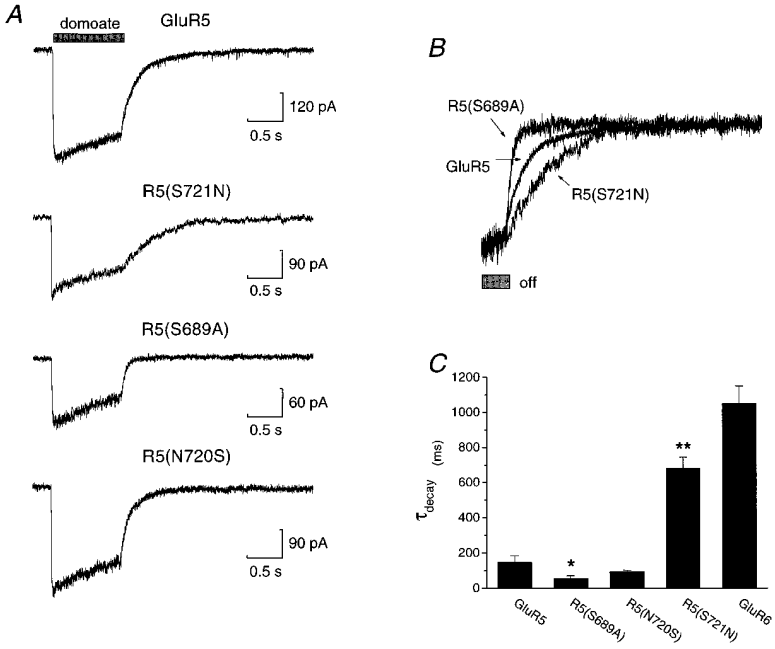

Figure 5. Domoate-Evoked Currents in GluR5 and Mutants (A and B) and Comparison of Deactivation Rates for GluR5, R5(S689A), R5(N720S), R5(S721N), and GluR6 (C)

(A) Currents evoked by application of 30 μM domoate to HEK cells expressing GluR5, R5(S721N), R5(S689A), and R5(N720S). The holding potential was −70 mV in each case.

(B) Comparison of deactivation rates after removal of domoate from GluR5, R5(S689A), and R6(S721N) traces shown in (A). The deactivation rate constants for the currents shown were 45 and 189 ms for R5(S689A), 166 and 754 ms for GluR5, and 481 ms and 11.5 s for R5(S721N).

(C) Plot of the mean fast deactivation rate constant for GluR5, the mutants shown in (A), and GluR6. Error bars indicate the SEM. A single asterisk denotes statistically significant difference from GluR5 of $p < 0.05$, and a double asterisk denotes a significance of $p < 0.001$. See Table 1 for the number of cells for each receptor.

and a mutant with normal kinetics, R5(N720S). The decay currents after removal of agonist are isolated and normalized in Figure 5B to compare directly their time courses. Deactivation of R5(S721N) after removal of domoate were in most cases best fitted with a single exponential with a $\tau = 0.55 \pm 0.02$ s (n = 5). One R5(S721N) cell could only be fitted with the sum of two exponential components, with $\tau_1 = 0.17$ s and $\tau_2 = 1.48$ s (68% and 32% of the current, respectively). We compared this single-exponential deactivation to the faster (and predominant) deactivation component of GluR5, the other GluR5 mutants, and GluR6. As shown in Figure 5C, the R5(S721N) deactivation rate is significantly slower than predominant deactivation component of GluR5 and the two other GluR5 mutants but still somewhat faster than the predominant deactivation rate for GluR6. It should be noted that R5(S721N) domoate currents were smaller than those from GluR5, and our ability to measure the deactivation rate was hampered by current noise in a similar manner to chimera R5tm1R6. We therefore cannot rule out the possibility that R5(S721N) may have a slower, unresolved exponential component in the current deactivation. Despite this uncertainty, these data demonstrate that mutation of R6(N721) and R5(S721) had at least partially reciprocal effects on domoate currents in GluR5 and GluR6.

Interestingly, mutation of S689 in GluR5 increased the rate of domoate current deactivation (predominant $\tau = 56 \pm 15$ ms; n = 7; see Figure 5); this contrasts with the lack of effect on deactivation rates after mutation of the corresponding amino acid in GluR6 (A689). In the double mutant R5(S689A/S721N), for which deactivation was best fitted with a single exponential component, domoate deactivation rates were not significantly different than native GluR5 ($\tau = 0.26 \pm 0.09$ s; n = 4), indicating that both sites may play a role in determining the current deactivation rate in GluR5 or that there may be other interacting residues.

Slowing of Kainate Desensitization Rates with Mutation of Amino Acid A689

Unlike AMPA sensitivity and domoate deactivation rates, no single amino acid mutation in the M3-M4 linker region of GluR6 altered the kainate-activated current desensitization properties to a rate resembling that of GluR5. However, mutation of A689 to a serine residue generated a channel with a significantly slower desensitization rate during application of kainate. Figure 6A shows examples of kainate applications to GluR6, R6(A689S), R6(N721S), and R6(A689S/N721S). In R6(A689S), desensitizing kainate currents were best fitted with the sum of two exponential components with $\tau_1 = 8.7 \pm 2.2$ ms and $\tau_2 = 108 \pm 36$ ms (proportionally 92% and 8% of the exponential decay, respectively; n = 6). The activation rate for R6(A689S) with kainate was indistinguishable from that of GluR6 (10%–90% rise time of 1.4 ± 0.1 ms for both receptors). The effect of this mutation on current properties is specific for kainate, as R6(A689S) responses to domoate and glutamate were similar to native GluR6 (see Figure 4 and Table 1). Furthermore, addition of a mutation at N721 does not alter the slower kainate desensitization of R6(A689S), as the double mutants R6(A689S/N721S) had kainate responses similar to those of R6(A689S): $\tau_1 = 8.1 \pm 0.9$ ms and $\tau_2 = 61 \pm 12$ ms (n = 8) (Figure 6B). These results demonstrate that mutation of A689 in GluR6 specifically affects the kainate response, while mutation of N721 alters the response to domoate and AMPA.

One other GluR6 mutant had an altered kainate desensitization rate as compared to wild type—R6(F735L) (Figure 6B). This mutant receptor had a $\tau_{des} = 6.8 \pm 0.7$ ms with kainate, which was significantly different from GluR6 ($p < 0.005$; n = 11). It is possible that the slower desensitization rates seen with this mutant reflect an alteration in the concentration dependence of the responses, as the current amplitudes with R6(F735L) are roughly half that of GluR6. Furthermore, the activation

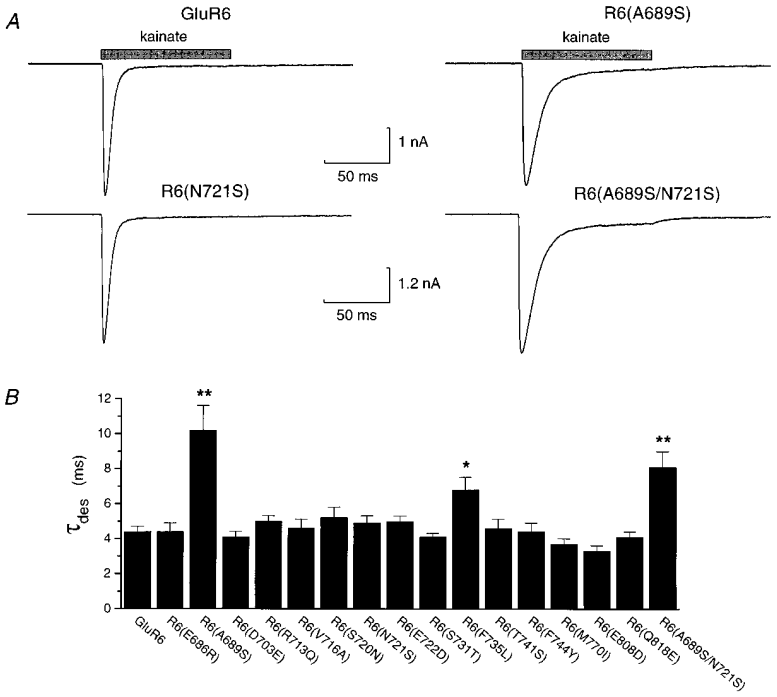

Figure 6. Kainate-Evoked Currents in GluR6 and Selected Mutants (A) and Comparison of Desensitization Rates for GluR6 and All R6 Mutants (B)

(A) Currents evoked by application of 1 mM kainate to HEK cells expressing GluR6, R6(A689S), R6(N721S), and R6(A689S/N721S). The holding potential was −70 mV in each case.

(B) Plot of the mean desensitization rates for GluR6 and R6 mutants shown in (A). Error bars indicate the SEM. A single asterisk denotes statistical significance of $p < 0.05$, and a double asterisk denotes a significance of $p < 0.001$. See Table 1 for the number of cells for each receptor.

rates are slower in R6(F735L) as compared to GluR6 (1.7 ± 0.1 ms versus 1.4 ± 0.1 ms for GluR6; n = 11 and 12, respectively). Since the effects on domoate deactivation rates and the kainate desensitization rates are not as substantial with this mutant as with R6(A689S) and R6(N721S), and R6(F735L) does not gate AMPA currents, the role that this residue plays in ligand binding and gating is unclear. However, it is possible that a more detailed examination of this particular mutant may prove interesting.

Effects of A689 and N721 Mutations on [^{3}H]Kainate Binding

In order to determine if the selectivity in agonist function is reflected by selectivity in agonist binding, the binding properties of R6(A689S) and R6(N721S) were examined. Previously reported K_D values for kainate binding to GluR6 have ranged from 13 nM (Tygesen et al., 1995) to 100 nM (Stern-Bach et al., 1994) (in different expression systems). In HEK 293 cells, the kainate affinity for GluR5 is lower than that for GluR6 (GluR5 K_D = 73 nM; GluR6 K_D = 36 nM) (Lomeli et al., 1992). K_i values for other agonists are generally similar between GluR5 and GluR6; the greatest differences are found in the K_i values for domoate (4-fold less potent on GluR6) and the lack of displacement by AMPA on GluR6 (Lomeli et al., 1992).

We first assayed the binding properties of wild-type GluR6, which seemed necessary given the variability in reported affinities. As shown in Figure 7 and Table 2, kainate had a K_D of 13.1 ± 1.7 nM (n = 3) in our assays, and K_i values for domoate and glutamate were 10.7 ± 2.9 nM (n = 4) and 556 ± 150 nM (n = 3), respectively. AMPA gave very little displacement of [^{3}H]kainate from GluR6 (<25% displacement at 250 μM; n = 3). These values are similar to those reported by Lomeli et al. (1992), with the exception of the K_D for kainate, which was somewhat lower than they reported (36 nM; Lomeli et al., 1992).

Mutation of A689 and N721 in GluR6 reduced the kainate-binding affinity by approximately 2- and 5-fold, respectively, and altered displacement by glutamate, domoate, and AMPA to different degrees (Figure 7). For R6(A689S), the K_D for kainate was 29.1 ± 4.5 nM, and the K_i values for domoate and glutamate were 7.7 ± 4.3 nM (n = 3) and 239 ± 49 nM (n = 3), respectively. As with GluR6, AMPA gave very little displacement of [^{3}H]kainate from R6(A689S) (<25% displacement at 250 μM; n = 3). For R6(N721S), the K_D for kainate was 62.0 ± 10.6 nM, and the K_i values for domoate and glutamate were 27.4 ± 1.3 nM and 214 ± 72 nM (n = 3 and 4, respectively). AMPA displaced [^{3}H]kainate binding to R6(N721S) with a K_i value of 16 ± 6 μM. Therefore, these binding results correlate with the most striking functional effect of the R6(N721S) mutation, generation of AMPA sensitivity. The fact that the measured R6(N721S) K_i of 16 μM does not entirely match the AMPA affinity for GluR5 (3 μM) may reflect the presence of additional sites that affect the AMPA-binding affinity or may be a result of inaccuracy in the analysis of this low affinity site.

Discussion

By making single amino acid substitutions between GluR5 and GluR6 and recording the agonist-evoked currents with high resolution, we have identified two amino acids that control aspects of the binding and functional responses of these kainate receptors. Mutation of asparagine 721 in GluR6 to a serine, the corresponding residue in GluR5, created an AMPA-sensitive GluR6 receptor that also had a domoate deactivation rate indistinguishable from that of GluR5. Mutation of all other residues

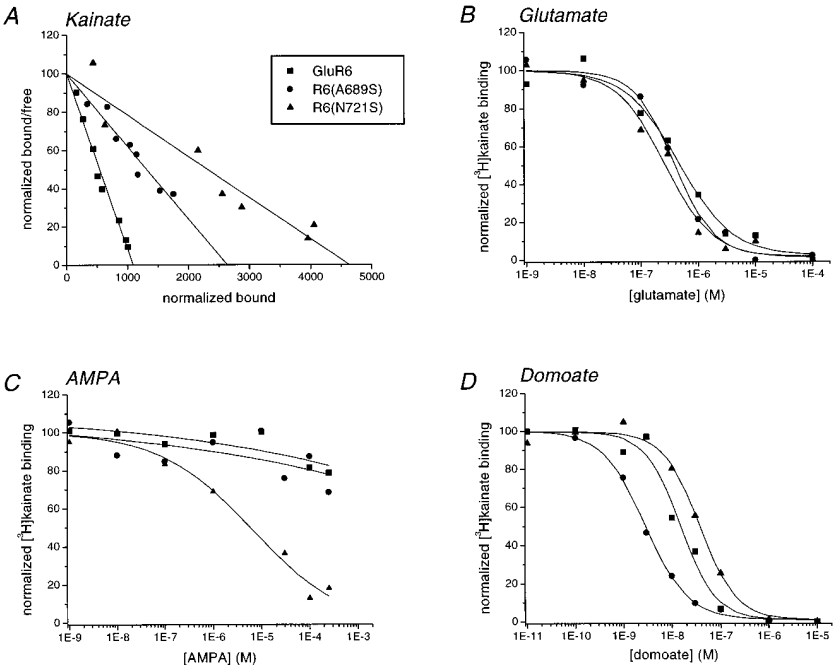

Figure 7. Binding Properties of GluR6, R6(A689S), and R6(N721S)

(A) Representative Scatchard plots calculated from the [^{3}H]kainate-binding isotherms using membranes prepared from HEK cells expressing GluR6 (closed squares), R6(A689S) (closed circles), and R6(N721S) (closed triangles). Nonspecific binding was determined in the presence of 100 μM kainate. Scatchards were normalized on both axes to facilitate comparison of binding affinities.

(B) Representative glutamate displacement curves for the three receptors.

(C) Representative AMPA displacement curves for the three receptors.

(D) Representative domoate displacement curves for the three receptors. In the displacement experiments, the concentration of [^{3}H]kainate was 5 nM for GluR6 and R6(A689S) and 10 or 15 nM for R6(N721S). Mean K_D and K_i values are given in Table 2.

that differed between GluR5 and GluR6 in the extracellular region between M3 and M4 had no effect on the AMPA sensitivity of the GluR6 channels, suggesting that these functional alterations are unlikely to be due to gross disruption of the tertiary structure of the protein. Additionally, mutation of alanine 689 to serine markedly slowed GluR6 desensitization rates. Mutation of N721 decreased the binding affinities of kainate and domoate, had a slight effect on glutamate affinity, and markedly increased AMPA sensitivity. In contrast, mutation of A689 selectively reduced kainate-binding affinity but had no significant effect on the affinity for domoate, glutamate, or AMPA. We therefore conclude that these amino acids are involved in the receptor-specific response to different agonists. Our results provide further insight into the structural makeup of the agonist-binding domain of ionotropic glutamate receptors.

Comparison with Previous Structure–Function Studies

Our current study complements and extends previous research on the structural components of ligand binding and function in a variety of glutamate receptor types. Previous site-mutation studies have used sequence homology with bacterial-binding proteins to localize a number of residues involved in ligand binding in AMPA receptors (Uchino et al., 1992; Li et al., 1995), NMDA

Table 2. Binding Properties of GluR5, GluR6, R6(A689S), and R6(N721S)

Receptor	[^{3}H]Kainate	Glutamate	Domoate	AMPA
GluR6				
Lomeli et al., 1992	36 ± 4.7	1080 ± 100	8.6 ± 1	>10,000
GluR6				
This study	13.1 ± 1.7	556 ± 150	10.7 ± 2.9	>>250,000
R6(A689S)	29.1 ± 4.5	239 ± 49	7.7 ± 4.3	>>250,000
R6(N721S)	62.0 ± 10.6	214 ± 72	27.4 ± 1.3	15,800 ± 6000
GluR5				
Lomeli et al., 1992	73 ± 19	290 ± 156	2.1 ± 0.8	3000 ± 1000

All receptors were expressed in HEK 293 cells, and binding properties were assayed as given in Experimental Procedures. Data from Lomeli et al., 1992, for GluR5 and GluR6 is given for the purpose of comparison. Kainate values are mean K_D ± SEM and are given in nM. The K_i values for glutamate, domoate, and AMPA are also in nM. For each mean K_D or K_i value, the number of determinations in this study was either three or four.

receptors (Kuryatov et al., 1994; Wafford et al., 1995; Hirai et al., 1996; Laube et al., 1997), and KBPs (Paas et al., 1996; Wo and Oswald, 1996). In a systematic attempt to localize important binding domains in a functional glutamate receptor, Stern-Bach and coworkers (1994) constructed a series of GluR3-GluR6 chimeras and assayed their pharmacological and binding properties in Xenopus laevis oocytes. The agonist pharmacology of their chimeras suggested residues in the N-terminal half of the S2 domain (S2N) were critical determinants of AMPA sensitivity between AMPA and kainate receptors. This interpretation was supported by an additional study with cross-family chimeras, in which replacement of the GluR2 S1 domain with a GluR6 S1 domain did not appreciably change the AMPA EC_{50} of the resultant chimera (Tygesen et al., 1995). We therefore tested whether residues in the S2 domain might similarly control the differential low affinity AMPA sensitivity that distinguishes GluR5 and GluR6. The functional properties of chimeras R6tm1R5 and R5tm1R6 (Figure 2) supported this idea, and we were further able to identify N721 as the amino acid that eliminated AMPA sensitivity in GluR6 as compared to GluR5. In AMPA receptor subunits, a threonine residue is conserved at the corresponding site in the proteins. Preliminary experiments with an additional GluR6 mutant, R6(N721T), and a GluR4 AMPA subunit mutant, R4(T708N), support the conclusions drawn in the current study. AMPA evoked currents of large amplitude from R6(N721T) (maximal currents at 500 μM AMPA were as large as 92% of the peak glutamate currents). Conversely, R4(T708N) showed reduced sensitivity to a number of agonists, including AMPA and glutamate (G. T. S., unpublished data). Interestingly, threonine is also conserved in the high affinity kainate receptor subunits KA-1 and KA-2, which coassemble with GluR5 and GluR6. Heteromeric GluR6/KA-2 channels are sensitive to AMPA, which gates with low potency a nondesensitizing current (Herb et al., 1992). Our results would suggest that the locus for this novel AMPA sensitivity conferred by KA-2 is T705. It is possible that there are additional sites necessary for the higher affinity AMPA binding, as has been proposed on the basis of sequence alignments of GluR1 and GluR6 (Sutcliffe et al., 1996).

Previous studies have also indicated that residues somewhere within the S2 domain appear to control receptor sensitivity to the high affinity agonist domoate (Stern-Bach et al., 1994; Tygesen et al., 1995). This is supported by the observation that a chimeric GluR6 receptor containing a GluR3 S2 domain [R6(R3S2)] had an EC_{50} 20-fold higher than that of wild-type GluR6 (Stern-Bach et al., 1994). In the present study, we have localized one S2 determinant of the functional response to domoate in kainate receptors. Within the kainate receptor family, there is also a significant difference in the domoate potency of the nondesensitized (peak) currents in GluR5 and GluR6. The peak EC_{50} for GluR5 has been reported as 1.2 μM (Sommer et al., 1992), while that of GluR6 is unknown but likely to be >50 μM (G. T. S., unpublished data). Despite a clear effect on deactivation rates, the relative peak responses for domoate versus glutamate or kainate were similar to those seen with GluR6. However, the degree of desensitization in R6(N721S) was greater than in GluR6; thus, the steady-state to peak current ratio with 30 μM domoate was 0.19 for R6(N721S) as compared to 0.42 for GluR6. The 3-fold reduced domoate-binding affinity for the R6 (N721S) receptor is consistent with the increased rate of decay of the currents after removal of domoate (see discussion in Wong et al., 1994). It should be noted, however, that in previous binding studies in HEK cells, the domoate affinity for GluR5 was higher than that of GluR6 (K_i for displacement of kainate 2.1 versus 8.6 nM, Lomeli et al., 1992). Thus, with respect to domoate binding, R6(N721S) behaves less like GluR5 (i.e., the affinity is lowered), whereas functionally this mutant exhibits GluR5-like deactivation kinetics. Our results therefore suggest that additional sites in these kainate receptors stabilize the higher domoate affinity observed with GluR5.

The current study also provides clear functional support for the importance of residues involved in kainate binding in KBPs (Paas et al., 1996) and validate the latter as useful constructs for modeling functional ionotropic glutamate receptors. Paas and coworkers identified several residues in both the S1 and S2 domains that accounted for the kainate-binding energy in these binding proteins, three of which are not conserved between GluR5 and GluR6: T102, S267, and Y299. The first amino acid is in the S1 domain, while the latter two are in the S2 domain and align with A689 and N721 in GluR6. S267A and Y299A mutations in chick KBP reduced the kainate-binding affinity by roughly 5-fold (Paas et al., 1996). In similar mutants for GluR6, R6(A689S) exhibited a 2-fold lower kainate-binding affinity compared to GluR6, but no alterations in kainate displacement by glutamate, domoate, or AMPA (see Figure 7 and Table 2). These binding data, when considered along with the selective effect of mutant A689S on the kainate desensitization rate, strongly suggest that this residue is directly involved in the binding of kainate but not the other agonists tested. In contrast, mutation of N721 in GluR6 altered binding affinities of kainate, domoate, and AMPA, but had detectable functional effects solely on the responses to domoate and AMPA. Kainate-binding affinities for R6(N721S) were reduced by 5-fold compared to GluR6, and the K_i value for domoate was decreased by 3-fold. Conversely, AMPA affinity was increased to a detectable level ($K_i = 15$ μM), although the sensitivity remained quite low (as is the case with GluR5; Sommer et al., 1992).

A Model of the GluR6 S1-S2 Domains Based on the Glutamine-Binding Protein Structure

Structure–function studies of ionotropic glutamate receptors have supported a model of the agonist-binding domain that uses the resolved structures of bacterial amino acid–binding proteins as archetypes. Nakanishi and coworkers first noted a degree of sequence similarity between the newly cloned AMPA receptor subunits and the glutamine-binding protein (GlnBP) of Escherichia coli (Nakanishi et al., 1990). At the time, AMPA receptors were thought to have four transmembrane-spanning domains by analogy with other ligand-gated ion channels (Hollmann and Heinemann, 1994). This

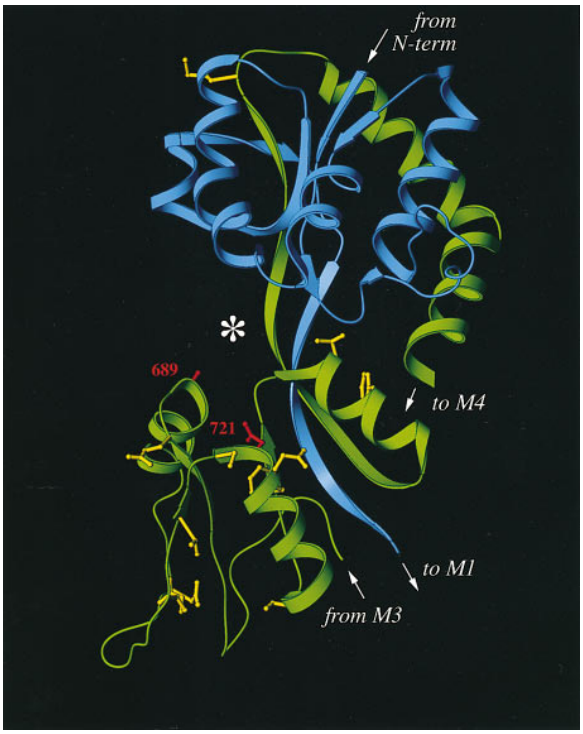

Figure 8. A Model for the GluR6 S1-S2 Binding Domains Based on the Resolved "Open" Structure of the Glutamine-Binding Protein (GlnBP)

This image was generated using the program SETOR (Evans, 1993). Secondary structure features are represented by flat ribbons (β strands) or coils (α helices). Regions with no corresponding amino acid in GlnBP were modeled independently by the Swiss-Model server (see Experimental Procedures). The S1 and S2 domains are colored blue and green, respectively. The side chains of A689 and N721 are colored red; other amino acids that differ between GluR5 and GluR6 are shown colored yellow. The asterisk marks the putative agonist-binding cleft. The orientation of the structure with respect to the membrane is unknown.

topology model placed the S1 and S2 domains on opposite sides of the plasma membrane. However, subsequent analysis of the N-glycosylation patterns of goldfish KBPs (Wo and Oswald, 1994), engineered sites in GluR1 (Hollmann et al., 1994), and inserted glycosylation sites and epitope fusion in GluR3 (Bennett and Dingledine, 1995) provided strong evidence for an alternate topology that modeled the classically defined M2 as a reentrant loop. Concurrently with these studies, Stern-Bach et al. (1994) demonstrated that the regions of receptor homology with bacterial periplasmic-binding proteins were clearly involved in ligand binding in GluR3-GluR6 chimeras.

To understand better the roles of the residues we mutated, we have generated a model of the GluR6 S1 and S2 domains based on the recently published crystallographic structure of unliganded GlnBP (Figure 8) (Hsiao et al., 1996). Previously published models of the glutamate receptor S1-S2 domains have relied on the structure of the lysine-arginine-ornithine binding protein (LAOBP) (Stern-Bach et al., 1994; Paas et al., 1996; Sutcliffe et al., 1996; Laube et al., 1997). While LAOBP shares significant sequence homology with GlnBP, it has only weak similarity to ionotropic glutamate receptors. Use of the GlnBP structure produced better initial sequence alignments and should make our model closer to the true GluR6 structure and therefore a more useful predictive tool.

Consistent with our functional results, GluR6 A689 and N721 are localized to α helices lining the agonist-binding pocket (Figure 8). Their appropriate localization therefore lends support to the idea that these residues form a direct interaction with ligands, rather than simply disrupting the tertiary structure of the protein. Other residues mutated in this study were distributed throughout the structure and were located further from the binding pocket. Analogous residues (S267 and Y299) in the chick KBP model based on LAOBP (Paas et al., 1996) are also located near the binding pocket in that structure. In the GluR6 model shown in Figure 8, S1 and S2 intertwine to form a bilobate structure common to most of the periplasmic binding proteins (Hsiao et al., 1996). The ligand-binding pocket is formed by central cleft of ~12 Å between the small and large lobes, which are connected by a central "hinge" region (Hsiao et al., 1996). A number of residues, including those preceding S1 and at the C-terminal end of S2, are not present in the model in Figure 8 because they have no counterparts in GlnBP. As has been noted previously (Paas et al., 1996), the precise orientation of the bilobate structure with respect to the plasma membrane is uncertain because of these extra unmodeled residues preceding M1 and M4.

Crystallization of a number of bacterial periplasmic binding proteins in their liganded state has shown that the two lobes move together upon agonist binding (Sack et al., 1989; Oh et al., 1993). A similar conformational change has been proposed to occur in ionotropic glutamate receptors and to underlie functional phenomena such as agonist trapping and desensitization (Benveniste and Mayer, 1995; Mano et al., 1996). In LAOBP, whose structure has been solved in the open unliganded and closed liganded states, agonist appears to bind to the larger lobe first (Oh et al., 1993). Interestingly, Oh et al. (1993) suggest that rotation about the hinge occurs in the absence of ligand and that ligand binding primarily stabilizes the closed structure due to favorable interactions with the smaller lobe. If the binding domains of ionotropic glutamate receptors behave in a similar fashion, our observation that mutation of an S2 amino acid, N721, produces a novel sensitivity to AMPA in GluR6 suggests that channel gating (i.e., functional activity) occurs only when the two lobes have stabilized in the closed liganded state. Based on GluR1 site mutants, it has been suggested that agonist binding to the larger lobe mediates channel opening, and interaction with the smaller lobe produces desensitization (a "venus flytrap" model; Mano et al., 1996). Our observations support an alternative model in which activation and desensitization are kinetic states entered into subsequent to lobe rotation and agonist interaction with the smaller (predominantly S2) lobe.

Resolved structures for liganded GlnBP (in preliminary form, Hsiao et al., 1996) and LAOBP (Oh et al., 1993) and the extrapolated model for chick KBP (Paas et al., 1996) support the interpretation that A689 and N721 in GluR6 directly interact with glutamate receptor agonists

in the binding pocket. The residues that interact with glutamine in GlnBP were recently reported in a preliminary form (Hsiao et al., 1996). Residue G119 of GlnBP, which aligns with A689 in GluR6, was shown to hydrogen bond to the carboxyl group of glutamine. Interestingly, this glycine residue bonds to glutamine through the backbone nitrogen, which may explain why mutations at this site in GluR6 (this paper) and cKBP (Paas et al., 1996) had no effect on the binding affinity or functional response for glutamate. Furthermore, the observation that complementary mutations of this site (serine to alanine in cKBP and alanine to serine in GluR6) both selectively reduce the kainate-binding affinity of GluR6 and cKBP suggests that the side chain of this residue interacts with other sites on the receptor protein itself, rather than directly with the ligand. With respect to N721 in GluR6, the aligned residue in GlnBP does not directly interact with glutamine (Hsiao et al., 1996). This again is consistent with the model of cKBP based on LAOBP, in which the complementary site affected kainate- but not glutamate-binding affinity.

In summary, we have systematically examined the roles played by S2 residues in generating divergent agonist responses in GluR5 and GluR6 kainate receptors. Detailed investigation of receptor kinetic properties allowed us to identify functionally important amino acid residues. This information should prove useful in further attempts to dissect out structural correlates of function in these receptors.

Experimental Procedures

Construction of Chimeras and Site Mutants

The R6tm1R5 chimera was constructed using a PCR-based mutation protocol. The sense oligonucleotide primer for this chimera was based on the nucleotide sequence for amino acids 559–563 (LSPDI) from GluR6 followed by 564–571 (WMYVLLAC) from GluR5 and contained a silent EcoRV site at the codon for amino acid 563. The antisense primer was from nucleotides 2722–2749 of GluR5 and contained a new XhoI site in the 3′ untranslated region. The C-terminal GluR5 fragment was generated by PCR with the following conditions: 95°C for 2 min; 35 cycles of 95°C for 30 s, 55°C for 30 s, and 75°C for 2 min; with a final extension of 75°C for 2 min. We used 900 ng of GluR5 plasmid DNA template, 150 pmol of each primer, 200 μM dNTPS, and 2 U Vent polymerase (NEB, Beverly, MA). The PCR product was isolated from an agarose gel, digested with EcoRV and XhoI, and subcloned into the GluR6 cDNA cut at the same restriction sites. Chimera R5tm1R6 and all site mutants were constructed using a modification of the Quikchange system (Stratagene, La Jolla, CA). Complementary oligonucleotide primers containing the site of mutation and a diagnostic silent restriction site were synthesized on-site or by Genset (La Jolla, CA). Repeated extensions of the entire plasmid template were carried out under the following conditions: 95°C for 1 min and 20 cycles of 95°C for 30 s, 60°C for 1.5 min, and 68°C for 18 min with 100–300 ng template DNA, 125–250 ng each of primers, 250 μM dNTPs, and 2.5 U Pfu polymerase (Stratagene). A DpnI digest of the PCR mix was then carried out for 1.5 hr at 37°C, and competent DH5α were transformed using standard procedures. For R5tm1R6, silent NheI sites were added by mutation of nucleotides 1783 in GluR5 and 2013 in GluR6. The NheI-XbaI fragment of GluR6 was then subcloned into the same sites in GluR5 to create R5tm1R6. For site mutants, screening of candidate mutants was carried out by restriction digest with a diagnostic enzyme or by direct dideoxy sequencing. All positive site mutants and chimeras were sequenced in the region of interest to confirm the mutation. The entire coding regions of a number of clones [R6(A689S), R6(N721S), R6(F735L), R6(689/721), R5(S689A), and R5(S721N)] were sequenced to ensure that functional changes were not a result of random mutations by the Pfu polymerase. Both GluR6 and GluR5 cDNAs were contained in CMV promoter-containing plasmids and had a glutamine at the Q/R editing site. GluR5 was generously donated by Peter Seeburg and corresponded to the splice variant GluR5–2a from Sommer et al. (1992) (renamed GluR5a in GenBank database). The GluR5a cDNA did not contain the N-terminal insertion reported by Bettler et al. (1992). DNA sequencing of the cDNA verified this deviation from the GenBank database sequence for GluR5a. Also, ten other nucleotide sequences in the GluR5–2a clone differed from the GenBank sequence for GluR5a; these mismatches do not affect the interpretation of our current results.

Transfection and Electrophysiology

HEK 293 cells were maintained in DMEM media supplemented with 100 μg/ml penicillin, 100 μg/ml streptomycin, and 10% FCS. One day before transfection, cells were split to low density on glass coverslips coated with 100 μg/ml poly-D-lysine and collagen. Transfection of receptor cDNAs was by standard calcium-phosphate precipitation with 1 μg cDNA per coverslip for 3–8 hr at 37°C and 8% CO_2. All receptor subunits were cotransfected with a CD8 antigen-containing plasmid (0.2 μg/coverslip). Electrophysiological recordings were made 1–3 days after transfection. To facilitate identification of transfected cells, coverslips were incubated with polystyrene beads coated with anti-CD8 antibody (Dynal Inc., Lake Success, NY). Patch clamp recordings were made using an Axopatch 200B amplifier (Axon Instruments, Foster City, CA). Patch electrodes were thick-walled borosilicate glass (Warner Instruments, Hamden, CT) and had a final resistance of 2–4 MΩ after fire polishing. The internal solution was composed of 110 mM CsF, 30 mM CsCl, 4 mM NaCl, 0.5 mM $CaCl_2$, 10 mM HEPES, and 5 mM EGTA (adjusted to pH 7.3 with CsOH). The external bath solution contained 150 mM NaCl, 2.8 mM KCl, 1.8 mM $CaCl_2$, 1.0 mM $MgCl_2$, and 10 mM HEPES (pH was adjusted to 7.3 with NaOH). Drugs were applied through three-barrel glass tubing (Vitro Dynamics, Rockaway, NJ) that had been pulled to a internal barrel diameter of ~80 μm and mounted on a piezoceramic bimorph. The piezo bimorph was driven by TTL pulses from pClamp 6.03 software (Axon Instruments) fed through a stimulation–isolation unit (S-100, Winston Electronic Co., Millbrae, CA); rise times of measured junction potential jumps were <0.5 ms. Data were acquired directly to a computer and were analyzed off-line using pClamp software. Exponential decays were fitted with the Chebyshev or Simplex least-squares algorithms in Clampfit.

Membrane Preparation and Radioligand Binding Assays

Membranes were prepared from ten 6 cm dishes, containing a total of ~1×10^7 cells, 48–72 hr after transfection. The cells were washed twice with HEPES buffer (40 mM HEPES [pH 8.0], 100 mM NaCl) prior to removal with a cell scraper. All subsequent steps were performed at 4°C or on ice and using ice-cold buffers. The cells were harvested at low speed (4,000 × g for 15 min) and resuspended in 5 ml HEPES buffer without NaCl. The cells were lysed with 20 strokes in a hand-held Potter homogenizer and the membranes recovered by centrifugation (100,000 × g for 30 min). The homogenization and centrifugation steps were repeated a further two times. Membranes were resuspended in the same buffer and stored at −70°C.

For all radioligand-binding experiments, samples were incubated in HEPES buffer (10 mM, pH 8.0) containing [^{3}H]kainate (58 Ci/mmol, NEN, Wilmington, DE) in a final volume of 0.5 ml for 1 hr at 0°C. Nonspecific binding was defined as that not displaced by 100 μM kainate. For competition studies, 10 nM [^{3}H]kainate was used; concentrations ranged from 1 to 200 nM in the saturation experiments. Bound and unbound radioligands were separated by vacuum filtration onto GF/C or GF/B filters (Whatman, Maidestone, UK), presoaked for 1 hr in 0.1% polyethyleneimine (RBI, Natick, MA), followed by two 4 ml washes in ice-cold HEPES buffer. All assays were performed in triplicate. Results from saturation experiments were analyzed using Scatchard transformations, and competition curves were fitted to the Hill equation.

Generation of GluR6 S1-S2 Model

A sequence alignment between E. coli GlnH and rat GluR6 was initially generated in a multiple alignment with the rat GluR1-GluR5,

GluR7, NMDAR1, and NMDAR2a sequences using the PILEUP program from the University of Wisconsin GCG software package. This initial alignment was optimized manually. Two stretches of GluR6, S432 to G547 and P667 to G801, were minimally required to align with GlnH and were used to build the model. Model construction was performed in a two-step process by the Swiss-Model server (http://www.expasy.ch; Peitsch, 1996) using the interface provided by the Swiss-PDBViewer program (available from the same site). In the first step, the truncated GluR6 sequence was compared to a database of structures to find suitably homologous proteins. The only template returned by the server was that of GlnH (PDB accession 1ggg). The GluR6 sequence was then threaded into the GlnH structure using the Swiss-PDBViewer application and the alignment obtained previously. Gaps were inserted into the GlnH sequence at six points to obtain an optimal alignment. The GluR6 sequences unaligned as a consequence were from 568–577, 603–615, 677–680, 699–713, 732, and 739. The Swiss-Model server modeled these sequences independently. With the exception of residue S739, these regions were distal from the putative agonist-binding site. Three of the loops (677–680, 699–713, and 732) were at the base of the structure, where S1 ends and S2 starts. It is this region of the receptor through which agonist binding is likely to be communicated to the receptor pore. This initial model was sent to the server for refinement and the building of loop regions. The final model was returned from the server in the form of a pdb file.

Acknowledgments

The authors would like to thank Peter Seeburg for the GluR5–2a cDNA. We also thank Connie Maron, Jane Sullivan, Bob Petroski, Cheryl Rogers, Carson Whiting, and Max Nanao for helpful advice and technical assistance. Melissa Hartley and the Core Sequencing Facility at the Salk Institute carried out the DNA sequencing. This work was supported by an NRSA fellowship (#1 F32 GM 18717-01) to G. T. S., an NRSA fellowship (#5 F32 NS 10079-02) to R. W. G., a National Institute for Neurological Diseases and Stroke grant (#2 RO1 NS 28709-06) to S. F. H., and a McKnight Endowment Fund for Neuroscience grant to S. F. H.

Received July 16, 1997; revised August 26, 1997.

References

Bennett, J.A., and Dingledine, R. (1995). Topology profile for a glutamate receptor: three transmembrane domains and a channel-lining reentrant membrane loop. Neuron *14*, 373–384.

Benveniste, M., and Mayer, M.L. (1995). Trapping of glutamate and glycine during open channel block of rat hippocampal neuron NMDA receptors by 9-aminoacridine. J. Physiol. *483*, 367–384.

Bettler, B., Boulter, J., Hermans-Borgmeyer, I., O'Shea-Greenfield, A., Deneris, E.S., Moll, C., Borgmeyer, U., Hollmann, M., and Heinemann, S. (1990). Cloning of a novel glutamate receptor subunit, GluR5: expression in the nervous system during development. Neuron *5*, 583–595.

Brose, N., Huntley, G.W., Stern-Bach, Y., Sharma, G., Morrison, J.H., and Heinemann, S.F. (1994). Differential assembly of coexpressed glutamate receptor subunits in neurons of rat cerebral cortex. J. Biol. Chem. *269*, 16780–16784.

Bufler, J., Heckmann, M., Jahn, K., and Franke, C. (1997). Distribution of desensitization time constants of mouse embryonic-like nicotinic and homomeric GluR6 glutamate receptor channels. Neurosci. Lett. *221*, 173–176.

Egebjerg, J., Bettler, B., Hermans-Borgmeyer, I., and Heinemann, S. (1991). Cloning of a cDNA for a glutamate receptor subunit activated by kainate but not AMPA. Nature *351*, 745–748.

Evans, S.V. (1993). SETOR: hardware-lighted three-dimensional solid model representations of macromolecules. J. Molec. Graphics *11*, 134–138.

Heckmann, M., Bufler, J., Franke, C., and Dudel, J. (1996). Kinetics of homomeric GluR6 glutamate receptor channels. Biophys. J. *71*, 1743–1750.

Herb, A., Burnashev, N., Werner, P., Sakmann, B., Wisden, W., and Seeburg, P.H. (1992). The KA-2 subunit of excitatory amino acid receptors shows widespread expression in brain and forms ion channels with distantly related subunits. Neuron *8*, 775–785.

Hirai, H., Kirsch, J., Laube, B., Betz, H., and Kuhse, J. (1996). The glycine binding site of the N-methyl-D-aspartate receptor subunit NR1: identification of novel determinants of coagonist potentiation in the extracellular M3-M4 loop region. Proc. Natl. Acad. Sci. USA *93*, 6031–6036.

Hollmann, M., and Heinemann, S. (1994). Cloned glutamate receptors. Annu. Rev. Neurosci. *17*, 31–108.

Hollmann, M., Maron, C., and Heinemann, S. (1994). N-glycosylation site tagging suggests a three transmembrane domain topology for the glutamate receptor GluR1. Neuron *13*, 1331–1343.

Hsiao, C.-D., Sun, Y.-J., Rose, J., and Wang, B.-C. (1996). The crystal structure of glutamine-binding protein from Escherichia coli. J. Mol. Biol. *262*, 225–242.

Köhler, M., Burnashev, N., Sakmann, B., and Seeburg, P.H. (1993). Determinants of Ca^{2+} permeability in both TM1 and TM2 of high affinity kainate receptor channels: diversity by RNA editing. Neuron *10*, 491–500.

Kuryatov, A., Laube, B., Betz, H., and Kuhse, J. (1994). Mutational analysis of the glycine-binding site of the NMDA receptor: structural similarity with bacterial amino acid-binding proteins. Neuron *12*, 1291–1300.

Laube, B., Hirai, H., Sturgess, M., Betz, H., and Kuhse, J. (1997). Molecular determinants of agonist discrimination by NMDA receptor subunits: analysis of the glutamate binding site on the NR2B subunit. Neuron *18*, 493–503.

Lerma, J., Paternain, A.V., Naranjo, J.R., and Mellstrom, B. (1993). Functional kainate-selective glutamate receptors in cultured hippocampal neurons. Proc. Natl. Acad. Sci. USA *90*, 11688–11692.

Li, F., Owens, N., and Verdoorn, T.A. (1995). Functional effects of mutations in the putative agonist binding region of recombinant alpha-amino-3-hydroxy-5-methyl-4-isoxazolepropionic acid receptors. Mol. Pharmacol. *47*, 148–154.

Lomeli, H., Wisden, W., Köhler, M., Keinanen, K., Sommer, B., and Seeburg, P.H. (1992). High-affinity kainate and domoate receptors in rat brain. FEBS Lett. *307*, 139–143.

Mano, I., Lamed, Y., and Teichberg, V.I. (1996). A venus flytrap mechanism for activation and desensitization of alpha-amino-3-hydroxy-5-methyl-4-isoxazole propionic acid receptors. J. Biol. Chem. *271*, 15299–15302.

Mosbacher, J., Schoepfer, R., Monyer, H., Burnashev, N., Seeburg, P.H., and Ruppersberg, J.P. (1994). A molecular determinant for submillisecond desensitization in glutamate receptors. Science *266*, 1059–1062.

Nakanishi, N., Shneider, N.A., and Axel, R. (1990). A family of glutamate receptor genes: evidence for the formation of heteromultimeric receptors with distinct channel properties. Neuron *5*, 569–581.

Oh, B.H., Pandit, J., Kang, C.H., Nikaido, K., Gokcen, S., Ames, G.F., and Kim, S.H. (1993). Three-dimensional structures of the periplasmic lysine/arginine/ornithine-binding protein with and without a ligand. J. Biol. Chem. *268*, 11348–11355.

Paas, Y., Eisenstein, M., Medevielle, F., Teichberg, V.I., and Devillers-Thiéry, A. (1996). Identification of the amino acid subsets accounting for the ligand binding specificity of a glutamate receptor. Neuron *17*, 979–990.

Partin, K.M., Patneau, D.K., Winters, C.A., Mayer, M.L., and Buonanno, A. (1993). Selective modulation of desensitization at AMPA versus kainate receptors by cyclothiazide and concanavalin A. Neuron *11*, 1069–1082.

Patneau, D.K., Wright, P.W., Winters, C., Mayer, M.L., and Gallo, V. (1994). Glial cells of the oligodendrocyte lineage express both kainate- and AMPA-preferring subtypes of glutamate receptor. Neuron *12*, 357–371.

Peitsch, M.C. (1996). ProMod and Swiss-Model: internet-based tools for automated comparative protein modeling. Biochem. Soc. Trans. *24*, 274–279.

Puchalski, R.B., Louis, J.-C., Brose, N., Traynelis, S.F., Egebjerg, J.,

Kukekov, V., Wenthold, R.J., Rogers, S.W., Lin, F., Moran, T., et al. (1994). Selective RNA editing and subunit assembly of native glutamate receptors. Neuron *13*, 131–147.

Sack, J.S., Saper, M.A., and Quiocho, F.A. (1989). Periplasmic binding protein structure and function. Refined X-ray structures of the leucine/isoleucine/valine-binding protein and its complex with leucine. J. Mol. Biol. *206*, 171–191.

Sommer, B., Keinänen, K., Verdoorn, T.A., Wisden, W., Burnashev, N., Herb, A., Köhler, M., Takagi, T., Sakmann, B., and Seeburg, P.H. (1990). Flip and flop: a cell-specific functional switch in glutamate-operated channels of the CNS. Science *249*, 1580–1585.

Sommer, B., Burnashev, N., Verdoorn, T.A., Keinänen, K., Sakmann, B., and Seeburg, P.H. (1992). A glutamate receptor channel with high affinity for domoate and kainate. EMBO J. *11*, 1651–1656.

Stern-Bach, Y., Bettler, B., Hartley, M., Sheppard, P.O., O'Hara, P.J., and Heinemann, S.F. (1994). Agonist selectivity of glutamate receptors is specified by two domains structurally related to bacterial amino acid-binding proteins. Neuron *13*, 1345–1357.

Sutcliffe, M.J., Wo, Z.G., and Oswald, R.E. (1996). Three-dimensional models of non-NMDA glutamate receptors. Biophys. J. *70*, 1575–1589.

Tygesen, C.K., Jørgensen, M., and Andersen, P.H. (1995). The importance of two specific domains in ligand binding to the AMPA/kainate glutamate receptors GluR2 and GluR6. FEBS Lett. *363*, 184–188.

Uchino, S., Sakimura, K., Nagahari, K., and Mishina, M. (1992). Mutations in a putative agonist binding region of the AMPA-selective glutamate receptor channel. FEBS Lett. *308*, 253–257.

Wafford, K.A., Kathoria, M., Bain, C.J., Marshall, G., Le Bourdelles, B., Kemp, J.A., and Whiting, P.J. (1995). Identification of amino acids in the N-methyl-D-aspartate receptor NR1 subunit that contribute to the glycine binding site. Mol. Pharmacol. *47*, 374–380.

Wenthold, R.J., Trumpy, V.A., Zhu, W.S., and Petralia, R.S. (1994). Biochemical and assembly properties of GluR6 and KA2, two members of the kainate receptor family, determined with subunit-specific antibodies. J. Biol. Chem. *269*, 1332–1339.

Wilding, T.J., and Huettner, J.E. (1995). Differential antagonism of α-amino-3-hydroxy-5-methyl-4-isoxazolepropionic acid-preferring and kainate-preferring receptors by 2,3-benzodiazepines. Mol. Pharmacol. *47*, 582–587.

Wilding, T.J., and Huettner, J.E. (1997). Activation and desensitization of hippocampal kainate receptors. J. Neurosci. *17*, 2713–2721.

Wo, Z.G., and Oswald, R.E. (1994). Transmembrane topology of two kainate receptor subunits revealed by N-glycosylation. Proc. Natl. Acad. Sci. USA *91*, 7154–7158.

Wo, Z.G., and Oswald, R.E. (1996). Ligand-binding characteristics and related structural features of the expressed goldfish kainate receptors: identification of a conserved disulfide bond and three residues important for ligand binding. Mol. Pharmacol. *50*, 770–780.

Wong, L.A., Mayer, M.L., Jane, D.E., and Watkins, J.C. (1994). Willardiines differentiate agonist binding sites for kainate- versus AMPA-preferring glutamate receptors in DRG and hippocampal neurons. J. Neurosci. *14*, 3881–3897.